Applied Physics A (2018) 124:66
https://doi.org/10.1007/s00339-017-1494-0

Applied Physics A
Materials Science & Processing

Thickness-dependent magnetic and transport properties of $La_{0.5}Sr_{0.5}MnO_3$ thin films deposited by DC magnetron sputtering on the $LaAlO_3$ substrate

K. Yadav[1,3] · H. K. Singh[2] · K. K. Maurya[2] · G. D. Varma[1]

Received: 13 July 2017 / Accepted: 19 December 2017
© Springer-Verlag GmbH Germany, part of Springer Nature 2017

Abstract

Thickness-dependent structural, magnetic and transport properties of $La_{0.5}Sr_{0.5}MnO_3$ (LSMO) thin films have been studied. A series of the LSMO films with thickness 30, 60, 125 and 300 nm have been deposited on the $LaAlO_3$ substrate using DC magnetron sputtering. The paramagnetic to ferromagnetic transition at T_C is followed by antiferromagnetic ordering at T_N in all films. It is also found that all LSMO films have T_C lower than that of bulk LSMO. A small variation of T_C is observed on increasing the film thickness. However, T_N is found to rise with increase in the film thickness. The 60 nm-thick film shows a wide insulator to metal transition. The resistivity above 240 K of the films with various thicknesses is consistent with a small polaronic hopping conductivity. The polaronic formation energy E_A rises with the increase of the film thickness except for 60 nm thin film, where a small decline in E_A is observed. The correlation between observed structural, magnetic and electrical properties with the thickness of the films has been discussed in this paper.

1 Introduction

The perovskite manganites (bulk as well as thin films) have been widely studied [1–12]. The properties are considerably different in thin films than in bulk. The epitaxial strains are created due to a mismatch of the crystal lattice parameters of the film and substrate, due to imperfections of the substrate, different sintering and growth conditions and even on changing the thickness of the film [12–27]. The strain is linked to the structural, electronic and magnetic properties of the thin films [28–30]. The strain in the thin film produces a change in the Mn–O–Mn bond angle and bond distances [16]. The strain also enhances the Jahn–Teller (J–T) distortions that lead to a formation of an insulating phase [16, 31]. The value of Curie temperature (T_C) is enormously sensitive to the strain [7, 16, 32]. A change in 1% strain leads to a 10% shift in T_C [32]. The strain also suppresses the ferromagnetism (FM) and reduces the T_C with a decrease in the thickness of the film [21, 22, 33–36]. The strain also relaxes on increasing the film thickness. It leads to the formation of misfit dislocations. Relaxation of a large amount creates more defects in the thin films. Oxygen deficiency is the most common defect that affects the physical properties of the thin film. Recently, the effect of oxygen annealing atmosphere on magnetic and dielectric properties has been reported [10, 37–39].

The bulk $La_{0.5}Sr_{0.5}MnO_3$ (LSMO) has been studied by many researchers. Charge ordering (CO) is observed in LSMO [40]. Fujishiro et al. reported T_C at 310 K and T_N at 150 K, but no metal–insulator (M–I) transition was observed [41]. However, Jirak et al. reported that T_N occurs at 220 K [42]. Some other researchers have also reported T_C at 320 K in LSMO [43] and T_N at 180 K [40]. It has also been reported by others that no CO occurs in LSMO [44–46]. The reason for the different properties reported in LSMO is still under debate. Some researchers have also studied the effect of the thin film thickness on the properties of $La_{0.5}Sr_{0.5}MnO_3$ [47–50]. But still, the effect of film thickness on magnetic and transport properties of the LSMO thin film is unclear.

In this paper, the LSMO ($x = 0.5$) films on $LaAlO_3$ (LAO) substrate have been deposited by the sputtering technique of

✉ K. Yadav
kamlesh.yadav001@gmail.com; kamlesh_yadav@cup.ac.in

[1] Department of Physics, Indian Institute of Technology, Roorkee 247667, India

[2] National Physical Laboratory, Dr. K. S. Krishnan Marg, New Delhi 110012, India

[3] Present Address: Department of Physical Sciences, School of Basic and Applied Sciences, Central University of Punjab, Bathinda 151001, India

Published online: 27 December 2017

the thicknesses ranging from ~30 to 300 nm. The magnetic and transport properties of LSMO thin films are investigated. The correlations between the structural, magnetic and transport properties of the LSMO films with the thickness have been discussed in this paper.

2 Experimental details

Thin films of $La_{0.5}Sr_{0.5}MnO_3$ with thickness ~30, 60, 125 and 300 nm were deposited by the DC magnetron sputtering technique on single crystal LAO substrates. The target was prepared by the standard solid-state reaction route from high purity La_2O_3, $SrCO_3$ and MnO_2 powders. The sputtering parameters such as the DC power, the substrate–target distance and the gas pressure were optimized to yield an average film thickness of ~ 6 nm per minute [51]. Prasad et al. [51] provide details of the deposition conditions. After deposition, the films were kept at 800 °C for half an hour at Ar (80%) + O_2 (20%) gas pressure of 1.0 Torr. Then the samples were slowly cooled down to room temperature for more than 3 h. All films were annealed at 750 °C under oxygen for 12 h to make the suitable oxygen stoichiometry compounds. The structural characterization of the samples was performed using an X-ray diffraction (XRD) θ–2θ (Bruker AXS D-8 advance); CuK (radiation) technique at room temperature and the rocking curve measurements were performed by a high-resolution XRD. The magnetization measurements were done using a SQUID magnetometer (MPMS XL Quantum). Resistivity as a function of temperature was measured by a standard four-probe method using Keithley instruments up to liquid He temperature.

3 Results and discussions

Figure 1 shows the X-ray diffraction (XRD) patterns recorded at room temperature of the films of thickness ~30 and 300 nm. The XRD for all the films shows the peaks of LSMO as in Fig. 1. We have calculated the out-of-plane lattice parameters of thin films from the (00λ) peaks. The out-of-plane unit cell lattice parameters are c = 3.867, 3.870 and 3.876 Å, respectively, for 30, 125 and 300 nm thin films. A small increase in the value of c with the thickness of the film indicates a slight stress relaxation of the deposited thin films. It also indicates that the straining of the films is small. The crystal structure of the bulk LSMO target used for sputtering is orthorhombic (Pbnm symmetry) with the lattice parameters a = 5.442 Å ($a/\sqrt{2}$ ~ 3.8487 Å), b = 5.446 Å ($b/\sqrt{2}$ ~ 3.8515 Å) and c = 7.753 Å ($c/2$ ~ 3.8765 Å). These values are in excellent agreement with a Rietveld refinement of the same composition [52]. Thus, the average in-plane lattice parameter of the bulk target material is

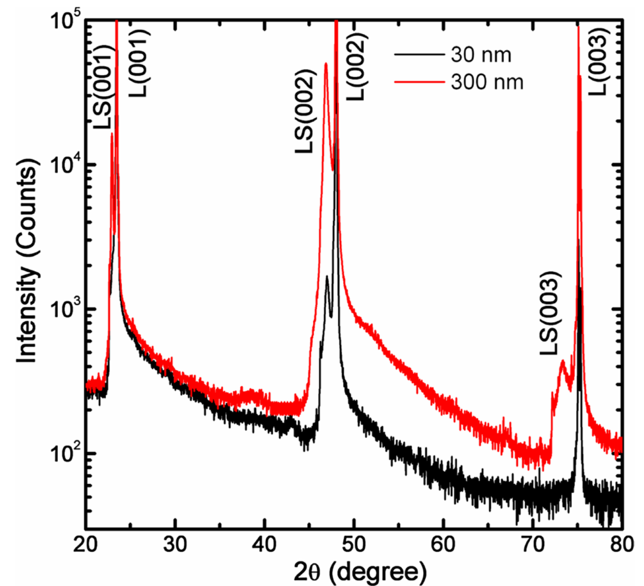

Fig. 1 X-ray diffraction (XRD) patterns, recorded at room temperature for 30 and 300 nm thin films of $La_{0.5}Sr_{0.5}MnO_3$

a_{av}=3.8501 Å, which is much larger than the value of the lattice constant of the substrate, which is 3.798 Å. Hence, the films are expected to grow under compressive strain. The large lattice mismatch leads to significant stresses and subsequently the formation of defects, which partly relieve the stress [53]. The existence of defects such as oxygen vacancies in $La_{0.5}Sr_{0.5}MnO_3$ thin films has been confirmed using X-ray photoelectron spectroscopy (XPS) by many researchers [54–56]. However, the out-of-plane lattice constants of the films are very close to the $c/2$ value for the bulk target. Leufke et al. recently reported that in the case of DC sputtering, the lattice parameters of the LSMO/STO films match with the bulk values [57]. We have also calculated the strain using the relation $\varepsilon = (\beta \cot\theta)/4$, as reported [58]. The values of the strain obtained for 30, 125 and 300 nm films are 2.4139×10^{-4}, 1.818×10^{-4} and 1.6810×10^{-4} respectively. It further confirms that there is strain relaxation with the increase in the thickness of the film. With the purpose of checking the crystalline nature of the films, $\theta - \omega/2\theta$ scans of all the films were done. Figure 2 shows $\theta - \omega/2\theta$ scans of a high-resolution XRD (HRXRD) for all the four samples with different thicknesses of ~30 to 300 nm. The values of the full width at half maximum (FWHM) are found to be nearly the same (~0.3) for all the films except for the 60 nm-thick film where the peak is little broadened. The peak broadening is due to the greater release of the strain in the LSMO epilayer in the 60 nm film. It results in the generation of more crystal defects in the film as compared to a 30 nm thin film. Almost the same FWHM of the rocking curves with the increase in the lattice relaxation implies that fewer defects are being generated as a consequence of the

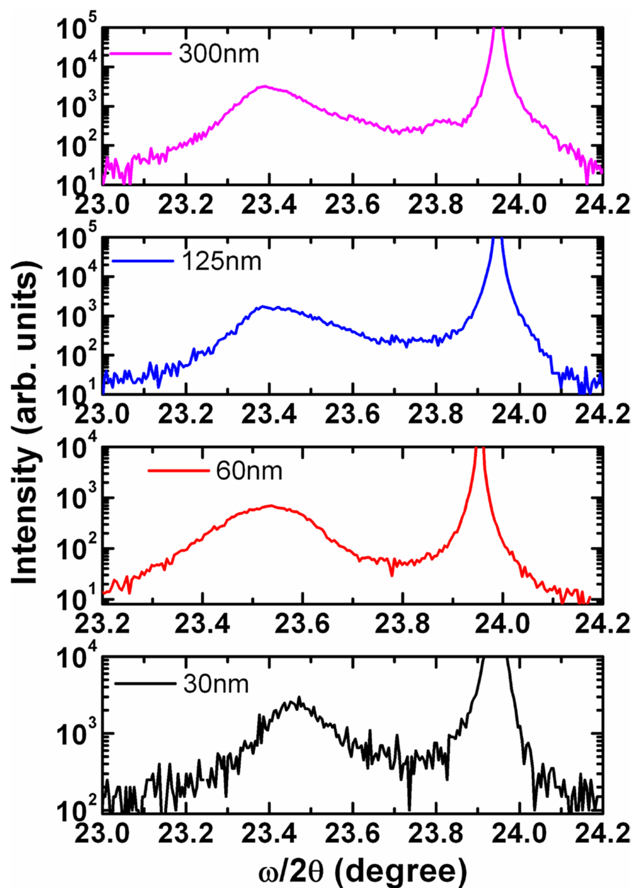

Fig. 2 $\theta - \omega/2\theta$ scans of the high-resolution XRD (HRXRD) for ~30, 60, 125 and 300 nm thin films of $La_{0.5}Sr_{0.5}MnO_3$

slight stress relaxation. Figure 3 shows a typical HRXRD pattern measured by the ω-scan for all the thin films. XRD analysis and rocking curve measurement show that all the films are coherently grown, have good crystalline quality and are epitaxial in nature.

The temperature-dependent magnetization (*M–T*) of the thin films, measured in the zero field cooled warming (ZFC) and the field cooled (FC) modes at applied magnetic field H = 100 Oe in the temperature range 300–4.2 K, is shown in Fig. 4a, b. From the *M–T* plot of 30 nm film, it can be seen that with a decrease in temperature below 300 K, the magnetization starts to increase and exhibit a typical PM–FM phase transition at ~235 K (T_C). On further lowering of the temperature, the magnetization decreases abruptly and the system enters into the AFM phase at a T_N ~150 K (Fig. 4a). The T_C and T_N are determined by taking the temperature corresponding to the minima and maxima in d*M*/d*T* vs. *T* plot, respectively. At the lowest temperature, a finite nonzero magnetic moment indicates the existence of the FM phase. Almost constant magnetic moment below ~75 K indicates the increase of the AFM phase below this temperature. Moreover, the *M–T* curve is irreversible and is indicated by the large bifurcation in the FC and the ZFC curves. The irreversibility between the ZFC and the FC magnetization curves starts just below T_C. The strong bifurcation could be a consequence of intense competition between the interactions that favor the AFM phase [e.g., JT effect and superexchange (SE)] and the DE that supports FM. The competition between the FM and the AFM interactions may lead to the formation of a cluster glass state [59]. The values of T_C are found to be ~235, 243, 240 and 236 K for 30, 60, 125 and 300 nm thin films, respectively. It shows that a small variation of T_C is observed with increase in the film thickness. It may be due to a small stress relaxation produced by the increase in the thickness of the films. It is also confirmed by the small variation of lattice parameters along the *c*-axis with the thickness of the films (see XRD results). The value of T_C for 60 nm thin film is higher than that for all the other films. It may be due to the production of a higher number of defects due to the significant stress relaxation in 60 nm thin film, as also evident from the XRD results. This result clearly shows that a significant stress relaxation is achieved up to film thickness 60 nm. Therefore, it leads to a large change in the properties at a film thickness of 60 nm. But, the most striking feature of *M–T* is the large reduction of T_C as compared to T_C ~ 310 K of the bulk sample [41]. The observed decrease of T_C of the films as compared to that of the bulk can be explained by taking the effect of the large lattice mismatch, as evident from the XRD results. It induces a larger distortion of the MnO_6 octahedron. This distortion enhances the JT distortion and causes an increase in the in-plane Mn–O–Mn bond distance and the Mn^{3+}–O–Mn^{4+} bond angle, which deviate more from the ideal value of 180°. Therefore, the in-plane transfer integral decreases. The oxidation states of Mn are 3 + and 4 +, which has been confirmed using XPS measurements of $La_{0.5}Sr_{0.5}MnO_3$ thin film by others [54–56]. Hence, the DE is significantly reduced and a reduction of T_C is observed in thin films with respect to bulk systems [60]. However, the possible causes of such large T_C reduction (~75 K) cannot be explained by the hopping integral alone. It is evident from the XRD results that a small stress relaxation occurs with the increase in the film thickness. Therefore, such a large change of T_C is not only due to the stress relaxation. These findings clearly indicate that all the films are also oxygen deficient, which may lead to the decrease of T_C. Oxygen deficiency leads to reduced connectivity of oxygen hopping between the transition metal ions. In other words, the indirect exchange (DE, SE) between magnetic cations mediated by the oxygen anions gets suppressed. In addition to this, the calculated values of T_N are ~150, 171, 160 and 165 K for 30, 60, 125 and 300 nm thin films, respectively. The T_N increases with increasing film thickness and the increase of T_N is relatively large (~21 K) for 60 nm thin films. The increase of T_N with the increase in the thickness of the thin film may be due to structural

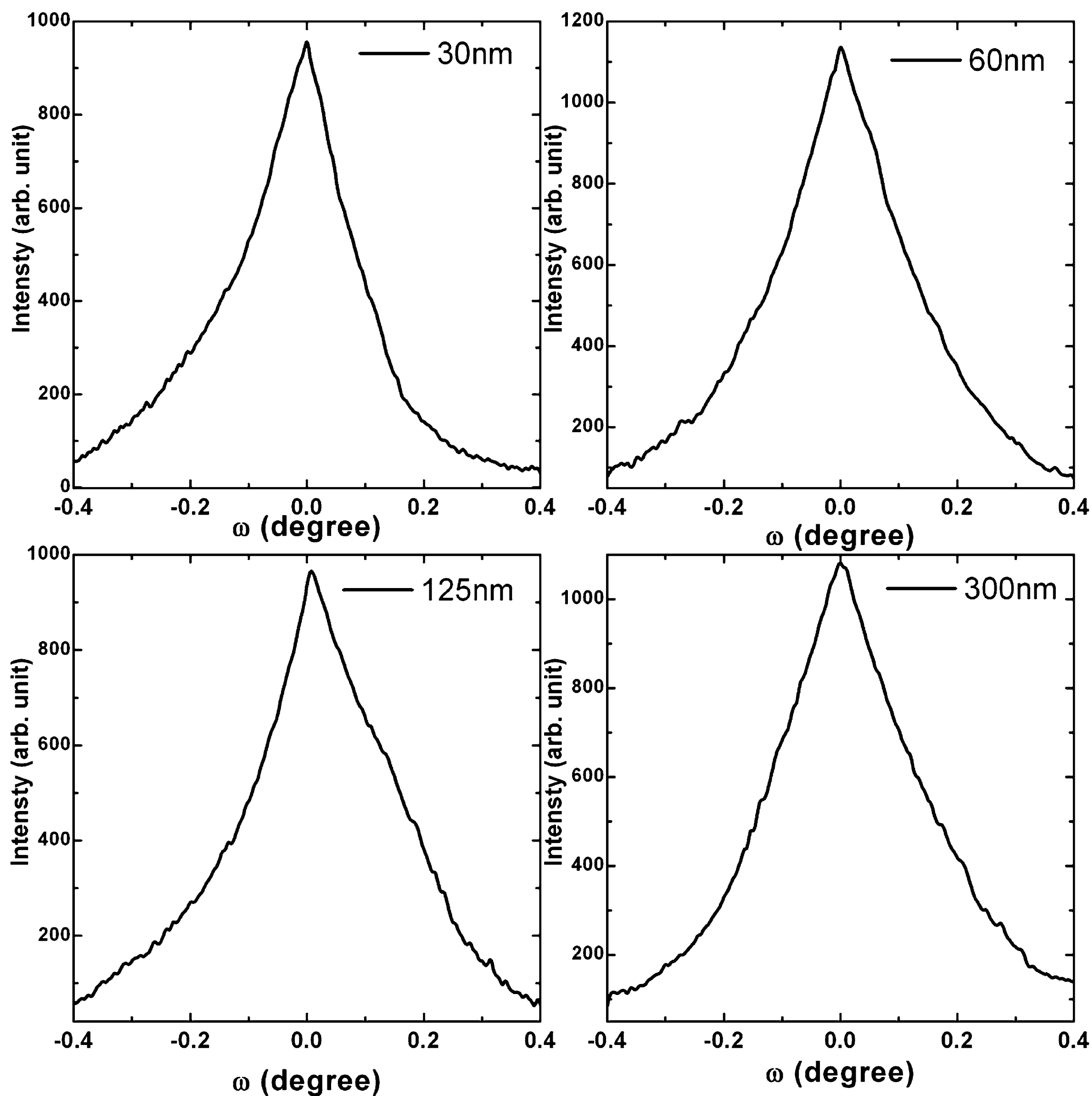

Fig. 3 ω scans of the high-resolution XRD (HRXRD) for ~30, 60, 125 and 300 nm thin films of $La_{0.5}Sr_{0.5}MnO_3$

disorders. Structural disorders can result in spin disorder and enhance electron scattering and localization. Also, large lattice mismatching leads to high stresses that afterward leads to the generation of various types of defects, such as tilting of grains, stacking faults and oxygen vacancies. The production of such defects may enhance the JT distortion in the localized regions, and hence an increase of T_N is observed. A relatively large increase of T_N by 21 K in 60 nm-thick film may be due to the higher density of defects that are produced in the film as the thickness increases above 30 nm, due to large stress relaxation as discussed [53]. But overall, no drastic change in the transition temperature is observed. This result is due to the production of a small strain due to the stress relaxation of the thin film with the increase in the thickness of the films, as also supported by the XRD results. The ZFC magnetization decreases with increase in the film thickness, except for the 60 nm thin film where a small increase in magnetization is observed (see Fig. 4). This result is again due to the creation of defects with increasing thickness that reduces the value of magnetization [33, 61, 62].

Figure 5 shows the temperature-dependent resistivity (ρ–T) of the LSMO films with different thicknesses ranging from 30 to 300 nm in the temperature range 300–4.2 K. The thin films show an insulating nature in the entire temperature range of the measurement. The resistivity keeps on increasing with the decrease of temperature. The resistivity increases rapidly with the decrease in the temperature below 70 K in all the thin films. It suggests that the role of the competing AFM interactions in the

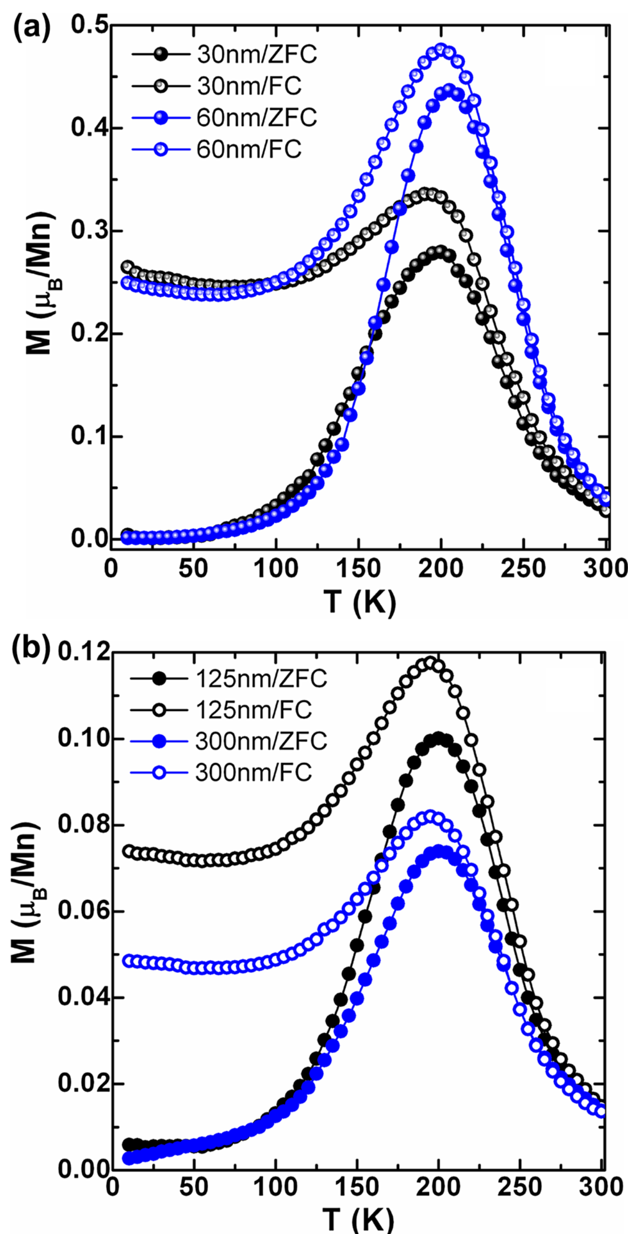

Fig. 4 The temperature-dependent magnetization (*M–T*) in the zero field-cooled warming (ZFC) and field-cooled (FC) modes at applied magnetic field H = 100 Oe for ~ 30, 60, 125 and 300 nm thin films of $La_{0.5}Sr_{0.5}MnO_3$

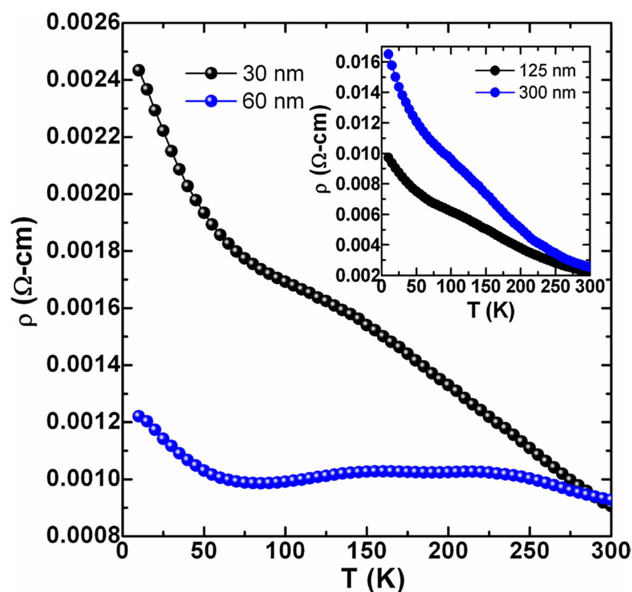

Fig. 5 The temperature-dependent resistivity (*ρ–T*) for ~ 30, 60, 125 and 300 nm thin films of $La_{0.5}Sr_{0.5}MnO_3$

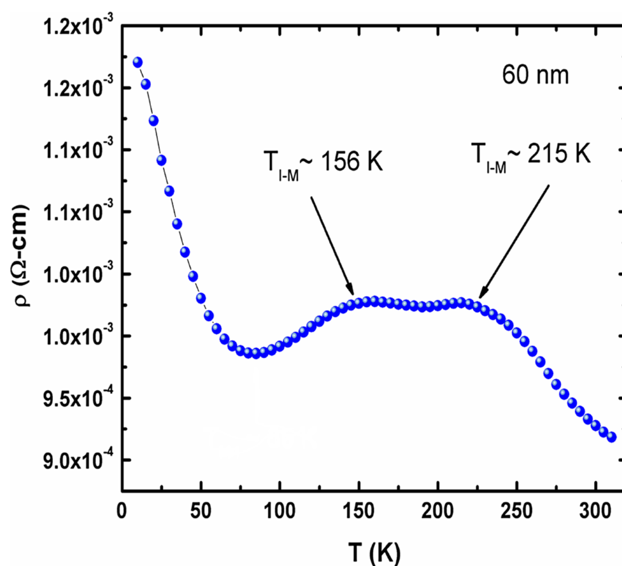

Fig. 6 The temperature-dependent resistivity (*ρ–T*) for a ~ 60 nm thin film of $La_{0.5}Sr_{0.5}MnO_3$

phase-separated regions becomes very significant. Thus, just below 70 K, the fractions of the AFM insulating phase increases rapidly. It results in a sharper rise in the resistivity. The largest value of resistivity for 30 nm film is 2.4 m Ω cm at 4 K. This indicates the high quality of the film. Furthermore, the *ρ–T* plot for the ~ 60 nm film shows quite peculiar properties as shown in Fig. 6. A broad peak of resistivity appears at almost the same T_C. It consists of two insulator–metal (I–M) like transitions. The ground state of the film consists of the coexisting ferromagnetic-metallic (FMM) and antiferromagnetic-insulating (AFMI) phases. The compressive in-plane strain yields the AFMI ground state, while the strain-relaxed part induces the FMM ground state. The compressive in-plane strain favors the I–M transition due to the J–T distortion. It is well known that the compressive in-plane strain may reduce the in-plane Mn–O bond lengths and lengthen the MnO_6 octahedra. It reduces the DE interaction and enhances the J–T distortion [63]. Thus, the J–T

distortion may provide freedom for the occurrence of an I–M transition. However, for thicker films (> 60 nm), no such transition is observed. A decrease of the resistivity is observed as the thickness of the film is increased up to 125 nm. Moreover, the 300 nm-thick film exhibits some higher resistivity value than the 125 nm-thick film. The thickness dependence of the resistivity is discussed here and gives some evidence of the grain boundary scattering. The polycrystalline films are made of grains that are separated by the grain boundaries. The free carriers trapped in the grain boundaries create an energy barrier between the adjacent grains. As the thickness increases, the grain size increases indicating a reduction in the grain-boundary density. As a result of this, the barrier height decreases with increase in the grain size. All these factors lead to a reduction in resistivity with increase in the thickness of the thin films.

The ρ–T plot can be best fitted with a small polaron hopping conduction (SPC) model $\rho(T) = \rho_0 T\exp(E_A/k_B T)$ (above T_C) and a Mott's variable range hopping (VRH) model $\rho = \rho_o\exp(T_0/T)^{1/4}$ (below T_N), where all the symbols have the usual meanings [46]. E_A and T_0 increase with increase in the film thickness, except for a 60 nm thin film where a small decrease is observed (see Table 1). The variation of E_A as a function of film thickness can be understood in terms of the magnetic disorder caused by the phase separation and the oxygen vacancies. This disorder increases the localization effects that may lead to the enhancement of the polaronic potential barrier. Hence, an increase in the activation energy is observed. Also, the presence of the lattice defects enhances the JT distortion and, consequently, the carrier localization is strengthened, resulting in a larger value of the activation energy. The value of T_0 is a measure of the strength of the J–T distortion and is inversely related to the extent of the localized states. Therefore, the small increase in T_0 with the thickness of the film (except 60 nm film) suggests that the localization length decreases, which reduces the average hopping distance. This is also due to the increase in the formation of defects that are the consequences of stress relaxation.

Table 1 The values obtained by fitting the electrical data

Film thickness (nm)	T_0 (K) ($T < T_N$)	E_A (meV) ($T > T_C$)
30	0.426	21.40
60	0.355	14.40
125	1.574	24.18
300	3.430	26.91

4 Conclusions

The effect of the thickness of the thin film (~ 30, 60, 125 and 300 nm) on the structural, magnetic and transport properties of $La_{0.5}Sr_{0.5}MnO_3$ (LSMO) polycrystalline thin films has been studied. A small variation of T_C with the increase in the thickness of the film was observed. However, a considerable reduction of T_C as compared to the bulk sample was found. Small shifts of T_N toward higher temperatures with increase in the film thickness were also observed. A systematic reduction in resistivity, activation energy and Mott parameters was observed with increase in the film thickness. Clear relationships between the structural distortions, stress relaxation, magnetic and the transport properties with the thickness of the film have been established. The results are explained on the basis of strain-induced Jahn–Teller (J–T) distortion and the formation of oxygen vacancies and the other defects.

Acknowledgements Kamlesh Yadav is grateful to the Ministry of Human Resources and Development (MHRD), New Delhi, for the award of a fellowship during the doctoral program.

References

1. Y. Tokura *Colossal Magneto-Resistive Oxides* (Gordon and Breach, New York, 2000)
2. E. Dagotto, T. Hotta, A. Moreo, Phys. Rep. **344**, 1 (2001)
3. J.M.D. Coey, M. Viret, S.V. Molnar, Adv. Phys. **48**, 167 (1999)
4. C. Zener, Phys. Rev. **82**, 403 (1951)
5. P.W. Anderson, H. Hasegawa, Phys. Rev. **100**, 675 (1955)
6. P.G. de Gennes, Phys. Rev. **118**, 141 (1960)
7. A.J. Millis, P.B. Littlewood, B.I. Shraiman, Phys. Rev. Lett. **74**, 5144 (1995)
8. A.J. Millis, B.I. Shraiman, R. Mueller, Phys. Rev. Lett. **77**, 175 (1996)
9. K. Yadav, M.P. Singh, F.S. Razavi, G.D. Varma, Mater. Sci. Eng. B **177**, 1219 (2012)
10. K. Yadav, M.P. Singh, F.S. Razavi, G.D. Varma, Mater. Chem. Phys. **137**, 323 (2012)
11. W. Prellier, B.E. Rauwel, B. Mercey, C. Simon, M. Hervieu, B. Raveau, J. Phys. Chem. Solids **64**, 1665 (2003)
12. W. Prellier, P. Lecoeur, B. Mercey, J. Phys. Condens. Matter. **13**, R915 (2001)
13. H.L. Ju, K.M. Krishnan, D. Lederman, J. Appl. Phys. **83**, 7073 (1998)
14. Y. Takamura, R.V. Chopdekar, E. Arenholz, Y. Suzuki, Appl. Phys. Lett. **92**, 162504 (2008)
15. C.K. Xie, J.I. Budnick, W.A. Hines, B.O. Wells, J.C. Woicik, Appl. Phys. Lett. **93**, 182507 (2008)
16. A.J. Millis, T. Darling, A. Migliori, J. Appl. Phys. **83**, 1588 (1998)
17. M. Bibes et al., Phys. Rev. B **66**, 134416 (2002)
18. T. Kanki, H. Tanaka, T. Kawai, Phys. Rev. B **64**, 224418 (2001)
19. A.K. Pradhan, D.R. Sahu, B.K. Roul, Y. Feng, Appl. Phys. Lett. **81**, 3597 (2002)
20. X.J. Chen, S. Soltan, H. Zhang, H.-U. Habermeier, Phys. Rev. B **65**, 174402 (2002)
21. B. Vengalis, A. Maneikis, F. Anisimovas, R. Butkute, L. Dapkus, A. Kindurys, J. Magn. Magn. Mater. **211**, 35 (2000)

22. F.S. Razavi et al., Appl. Phys. Lett. **76**, 155 (2000)
23. C.A. Perroni, V. Cataudella, G. De Filippis, G. Iadonisi, V.M. Ramaglia, F. Ventriglia, Phys. Rev. B **68**, 224424 (2003)
24. M. Ziese, H.C. Semmelhack, K.H. Han, J. Appl. Phys. **91**, 9930 (2002)
25. X.J. Chen et al., Phys. Rev. B **72**, 104403 (2005)
26. F. Tsui, M.C. Smoak, T.K. Nath, C.B. Eom, Appl. Phys. Lett. **76**, 2421 (2000)
27. A.M. H-Gosnet, J.P. Renard, J. Phys. D Appl. Phys. **36**, R127 (2003)
28. H. Tanaka, T. Kawai, Phys. Rev. B **60**, 14163 (1999)
29. M. Izumi et al., Appl. Phys. Lett. **73**, 2497 (1998)
30. M. Bibes et al., Phys. Rev. Lett. **87**, 067210 (2001)
31. A. Asamitsu, Y. Tomioka, H. Kuwahara, Y. Tokura, Nature **388**, 50 (1997)
32. Q. Qian et al., Phys. Rev. B **63**, 224424 (2001)
33. J.Z. Sun, D.W. Abraham, R.A. Rao, C.B. Eom, Appl. Phys. Lett. **74**, 3017 (1999)
34. S. Jin, T.H. Tiefel, M. McCormack, R.A. Fastnacht, R. Ramesh, L.H. Chen, Science **264**, 413 (1994)
35. R. Prasad, H.K. Singh, M.P. Singh, W. Prellier, P.K. Siwach, A. Kaur, J. Appl. Phys. **103**, 083906 (2008)
36. R. Prasad, M.P. Singh, P.K. Siwach, A. Kaur, P. Fournier, H.K. Singh, Appl. Phys. A **99**, 823 (2010)
37. V. Katari, S.N. Achary, S.K. Deshpande, P.D. Babu, A.K. Sinha, H.G. Salunke, N. Gupta, A.K. Tyagi, J. Phys. Chem. C **118**, 17900 (2014)
38. F.N. Sayed, S.N. Achary, O.D. Jayakumar, S.K. Deshpande, P.S.R. Krishna, S. Chatterjee, P. Ayyub, A.K. Tyagi, J. Mater. Res. **26**, 567 (2011)
39. H.Z. Guo, A. Gupta, M. Varela, S.J. Pennycook, Appl. Phys. Lett. **91**, 202509 (2007)
40. S.I. Patil et al., Phys. Rev. B **62**, 9548 (2000)
41. H. Fujishiro, T. Fukase, M. Ikebe, J. Phys. Soc. Jpn. **67**, 1799 (1998)
42. Z. Jirák, J. Hejtmánek, K. Knízek, M. Marysko, V. Síma, R. Sonntag, J. Magn. Magn. Mater. **217**, 113 (2000)
43. G.H. Jonker, J.H.V. Santen, Phys. (Utrecht) **16**, 337 (1950)
44. D. Joonghoe, W.S. Kim, N.H. Hur, Phys. Rev. Lett. **87**, 187201 (2001)
45. D. Joonghoe, E.O. Chi, W.S. Kim, N.H. Hur, Y.N. Choi, Phys. Rev. B **65**, 132414 (2002)
46. Y. Moritomo, T. Akimoto, A. Nakamura, K. Ohoyama, M. Ohashi, Phys. Rev. B **58**, 5544 (1998)
47. B. Gharbage, F. Mandier, H. Lauret, C. Roux, T. Pagnier, Solid State Ion **82**, 85 (1995)
48. G.L. Yuan et al., Mater. Lett. **53**, 76 (2002)
49. E. Quenneville, M. Meunier, A. Yelon, F. Morin, J. Appl. Phys. **90**, 1891 (2001)
50. J.M. Liu et al., Phys. Rev. B **62**, 8976 (2000)
51. R. Prasad, A. Gaur, P.K. Siwach, G.D. Varma, A. Kaur, H.K. Singh, J. Phys. Condens. Matter. **40**, 2954 (2007)
52. R. Bindu, Eur. Phys. J. B **37**, 321 (2004)
53. B. Wiedenhorst et al., Appl. Phys. Lett. **74**, 3636 (1999)
54. P. Decorse, E. Quenneville, S. Poulin, M. Meunier, A. Yelon, F. Morin, J. Vac. Sci. Technol. **19**, 910 (2001)
55. T. Li, Y. Du, H. Yan, Int. J. Mod. Phys. B **20** 551 (2006)
56. Q.-H. Wu, M. Liu, W. Jaegermann, Mater. Lett. **59**, 1980 (2005)
57. P.M. Leufke et al., Thin Solid Films **520**, 5521 (2012)
58. A. Akl, A.S. Hassanien, Superlattices Microstruct. **85**, 67 (2015)
59. J.A. Mydosh, *Spin Glass: An Experimental Introduction*. (Taylor and Francis, London, 1993)
60. K. Steenbeck, T. Habisreuther, C. Dubourdieu, J.P. Senateur, Appl. Phys. Lett. **80**, 3361 (2002)
61. J. Aarts, S. Freisem, R. Hendrikx, H.W. Zandbergen, Appl. Phys. Lett. **72**, 2975 (1998)
62. R.A. Rao, D. Lavric, T.K. Nath, C.B. Eom, L. Wu, F. Tsui, J. Appl. Phys. **85**, 4794 (1999)
63. J. Zhang, H. Tanaka, T. Kanki, J.H. Choi, T. Kawai, Phys. Rev. B **64**, 184404 (2001)